Parameterization of tight-binding models from density functional theory calculations

A. Urban,[1] M. Reese,[2,3] M. Mrovec,[2,3] C. Elsässer,[2,3] and B. Meyer[1,*]

[1]*Interdisciplinary Center for Molecular Materials ICMM and Computer Chemistry Center CCC, Friedrich-Alexander University Erlangen-Nürnberg, Nägelsbachstraße 25, D-91052 Erlangen, Germany*

[2]*Fraunhofer Institute for Mechanics of Materials IWM, Wöhlerstraße 11, D-79108 Freiburg, Germany*

[3]*Institute of Applied Materials—Reliability of Components and Systems IAM-ZBS, Karlsruhe Institute for Technology KIT, Kaiserstraße 12, D-76131 Karlsruhe, Germany*

(Received 13 May 2011; revised manuscript received 26 July 2011; published 17 October 2011)

We present a rigorous bottom-up approach for the derivation of the electronic structure part of tight-binding (TB) models from density functional theory (DFT) calculations. The approach is based on a simultaneous optimization and projection of atomic-like orbitals on self-consistent DFT wave functions and is universally applicable to elements and compounds in arbitrary structural arrangements. The quality and transferability of the derived TB bond and overlap integrals are demonstrated for the examples of a covalent semiconductor (carbon), a transition metal (titanium), and a binary compound with mixed metallic-covalent bonding (TiC). The method can serve as a transparent and physically justified coarse-graining scheme for the construction of nonorthogonal and orthogonal TB total-energy models as well as the closely related bond-order potentials.

DOI: 10.1103/PhysRevB.84.155119 PACS number(s): 31.15.ae, 71.15.Ap, 71.15.Nc

I. INTRODUCTION

Density functional theory (DFT) has become a widely established tool for first-principles total-energy calculations of extended atomic ensembles.[1] The main advantage of DFT is its universal applicability to most elements in the periodic table and various bonding environments, ranging from atoms, molecules, and small clusters to condensed solid and liquid phases. DFT calculations are, however, computationally very demanding and therefore limited to rather small system sizes, short simulation times, and moderate configurational sampling. Many interesting phenomena occurring in complex structural arrangements (e.g., in amorphous phases, extended crystal defects, or flexible molecular assemblies) usually need to be studied by faster and more approximate simulation methods.

In many cases empirical interatomic potentials,[2–5] parameterized to reproduce a set of experimental or first-principles data, are able to provide valuable insight into the physical and chemical properties of complex systems. Unfortunately, such potentials often suffer from a poor transferability and their use is thus limited to structures and bonding environments similar to those explicitly included in the fitting procedure.

A convenient compromise between the accurate but demanding first-principles DFT approach and the fast but less reliable empirical interatomic potentials are approximate, semi-empirical quantum-mechanical techniques, such as the tight-binding (TB) method.[6] In TB, the electronic structure problem is, in principle, approached equivalently as in DFT by constructing a Hamiltonian of the system and solving for its eigenvalues and eigenfunctions. However, unlike solving the variational problem in a self-consistent manner using a large number of basis functions, TB assumes only a minimal local basis of atomic orbitals, and in its usual form it is non-self-consistent. The TB Hamiltonian is simplified and composed of parameterized distance-dependent bond (Slater-Koster) integrals[7] that represent interactions between the atomic s, p, and d orbitals centered on the atoms. By maintaining the quantum-mechanical description of the chemical bond, and thereby including the proper physics of interatomic interactions, the TB method provides an improved transferability compared to empirical interatomic potentials. At the same time, the approximations made (e.g., the use of a minimal atomic basis, non-self-consistency) enable faster computation times and to treat larger systems than in DFT methods.

The crucial quantities of all TB models—the bond and overlap integrals—are usually determined by fitting to reproduce either selected sets of experimental data (empirical TB) or calculated band structures and total energies from higher-level electronic structure methods (semi-empirical TB).[8–11] This fitting procedure of a rather large parameter set is an elaborate and tedious task, in particular in cases where more chemical elements have to be considered simultaneously. Since the success of a TB model in terms of accuracy and transferability is determined by its parameterization, more straightforward approaches that avoid or at least reduce the arbitrariness of fitting are highly desirable.

In principle, the bond and overlap integrals as a function of interatomic distance can be obtained directly from DFT calculations by utilizing a minimal basis of atomic orbitals. The crucial problem is, however, which minimal basis and which Hamiltonian to use. In the past, different approaches following such a route have been proposed, for instance, the density-functional tight-binding (DFTB) method,[12–15] or schemes based either on linear muffin-tin orbitals (LMTOs)[16–19] or quasi-atomic minimal-basis orbitals (QUAMBOs).[20–25]

In the DFTB method, the s, p, and d orbitals of a self-consistent DFT calculation for free, isolated atoms in a specifically chosen quadratic confinement potential are taken as the minimal basis of atomic orbitals.[12] With this fixed basis the bond and overlap integrals are derived from non-self-consistent dimer calculations, using a superposition of the atomic potentials as the dimer potential. This procedure yields two-center bond and overlap integrals, but it neglects the effect of three-center contributions and the crystal field

splitting in the on-site matrix elements that are both present in structures containing more than two atoms. The obtained bond and overlap integrals are only distance dependent and correspond to a dimer bonding environment.

With LMTOs or QUAMBOs chosen as a minimal basis, other atomic arrangements than dimers may be used to derive TB parameters. This allows to take into account the three-center contributions and environment dependencies of bond and overlap integrals. However, DFT calculations with a minimal LMTO basis are mostly limited to the so-called atomic sphere approximation (ASA), which restricts the reference configurations for calculating TB parameters to rather close-packed crystal structures. The QUAMBOs present the most flexible basis as they are derived in a post-processing step from the wave functions of self-consistent DFT calculation for arbitrary configuration. They are constructed to reproduce exactly the electronic structure information below a chosen energy threshold (typically the Fermi level). The QUAMBOs resemble regular atomic s, p, and d orbitals, but due to the requirement of exact reproducibility of the electronic structure (occupied subspace) they are not pure eigenfunctions of the angular momentum operator. Therefore, the Slater-Koster rules[7] for rotating the bond and overlap integrals are no longer applicable, and the QUAMBOs together with the resulting bond and overlap integrals have to be recalculated for each new local atomic environment which leads to a much higher numerical effort.[24]

In the present paper we present an alternative approach which allows to derive bond and overlap integrals for TB models directly from DFT calculations in a rigorous and well-defined way. Our new approach combines the advantages of the three earlier schemes. The method is based on a projection formalism[26,27] and a constrained search for a minimal basis of optimized atomic orbital functions. The atomic orbitals retain their s, p, or d character (as in the DFTB approach), so that the Slater-Koster rules still apply. However, the atomic orbitals are not kept fixed, but their radial functions are adjusted to give the best possible representation of the wave functions from the self-consistent DFT calculations for selected reference configurations. Since we retain our basis functions to be angular-momentum eigenfunctions, this representation is not exact (unlike in the QUAMBO approach), but only approximate (see "spillage" below). By allowing the atomic orbitals to adjust to different environments and by rotating the atomic orbitals, we include the information about the three-center contributions to the bond integrals in an averaged manner. Furthermore, crystal field splittings are also determined in our projection scheme and included in our TB models.

The major advantages of our new approach are that the bond and overlap integrals can be derived from any arbitrary (atomic, molecular, or crystalline) configuration, and that it is universally applicable to both elements and compounds. This enables us to test the transferability of TB parameters not only between different structural configurations but also in different chemical environments. In addition, our approach can be used as a convenient *coarse-graining* scheme that provides a well defined and physically transparent route from DFT via TB to interatomic potentials and atomistic linear-scaling (order-N) simulations.[28–30] Advanced interatomic potentials, such as bond-order potentials,[31–33] can be constructed with only a little effort provided that a reliable orthogonal TB parameterization exists. The simple and transparent approach is crucial, in particular for multicomponent systems since for both conventional TB methods and interatomic potentials, the number of model parameters explodes and the fitting becomes very tedious and ambiguous.

The paper is organized as follows. In Sec. II we briefly outline the TB method to establish our notation. Section III describes how nonorthogonal TB Hamiltonians are derived from DFT calculations. Procedures associated with the transformations between nonorthogonal and orthogonal TB Hamiltonians are discussed in Sec. IV. The summary and conclusions are given in Sec. V.

II. TIGHT-BINDING METHOD AND SLATER-KOSTER INTEGRALS

The formal relationship between the TB method and first-principles DFT has been established more than 20 years ago.[6,16,34–36] The total energy $E_{\rm tot}^{\rm TB}$ of an ensemble of atoms (for a nonmagnetic material) is approximated in TB as the sum of two contributions: a bonding many-body term and a sum of short-ranged repulsive pair potentials $\Phi_{\alpha\beta}$

$$E_{\rm tot}^{\rm TB} = \sum_{i}^{\rm occ} \varepsilon_i + \sum_{\alpha\neq\beta} \Phi_{\alpha\beta}(R_{\alpha\beta}). \tag{1}$$

$R_{\alpha\beta}$ is the distance between two atoms α and β at the positions $\mathbf{R}_\alpha$ and $\mathbf{R}_\beta$. The pair potentials account for the Coulomb repulsion between the ionic cores of the atoms and the double-counting corrections to the bond energy part for the electron-electron interaction and the exchange-correlation contribution to the total energy. The bonding many-body term is given as the sum of the energy eigenvalues ε_i of all occupied eigenstates ψ_i from a single-particle Schrödinger equation

$$\widehat{H}\,\psi_i(\mathbf{r}) = \varepsilon_i\,\psi_i(\mathbf{r}), \quad \widehat{H} = \widehat{T} + V_{\rm eff}^{\rm KS}(\mathbf{r}). \tag{2}$$

For the derivation of TB parameterizations using our projection scheme, the effective potential $V_{\rm eff}^{\rm KS}$ in the single-particle Hamiltonian $\widehat{H}$ is taken from the corresponding self-consistent DFT calculation. In TB, the single-particle Schrödinger equation is formally solved by expanding the wave functions ψ_i in terms of a minimal basis of atomic orbitals $\{\phi_\mu\}$

$$\psi_i(\mathbf{r}) = \sum_{\mu} c_\mu^i\,\phi_\mu(\mathbf{r}-\mathbf{R}_\alpha), \quad \mu = (\alpha,l,m). \tag{3}$$

With the single index μ we label all atomic orbitals centered at different atomic sites α and with orbital angular-momentum and magnetic quantum numbers l and m. This basis set expansion transforms the single-particle Schrödinger equation into a generalized matrix eigenvalue problem

$$\sum_{\nu} H_{\mu\nu}\,c_\nu^i = \varepsilon_i \sum_{\nu} S_{\mu\nu}\,c_\nu^i, \tag{4}$$

with the Hamilton and overlap matrix elements

$$H_{\mu\nu} = \langle\phi_\mu|\widehat{H}|\phi_\nu\rangle, \quad S_{\mu\nu} = \langle\phi_\mu|\phi_\nu\rangle. \tag{5}$$

In TB calculations, the elements of the Hamilton and overlap matrices are not calculated explicitly, but they are provided

in a parameterized form, typically as simple (analytical or numerical) one-dimensional functions of the distance between two atoms. With the submatrix for an atom pair being rotated into a bond-oriented coordinate system, the resulting integrals are usually termed $ss\sigma$, $sp\sigma$, $pp\sigma$, $pp\pi$, and so on, in the classical notation of Slater and Koster.[7]

TB models are further distinguished into nonorthogonal (NOTB) schemes, which contain an overlap matrix as in Eq. (4), and orthogonal (OTB) schemes, whose overlap matrix is the unity matrix. Nonorthogonal TB parameterizations can always be transformed into orthogonal ones by a suitable transformation, for instance, Löwdin's well-known symmetric orthogonalization[37]

$$\widetilde{\mathbf{H}} = \mathbf{S}^{-1/2}\,\mathbf{H}\,\mathbf{S}^{-1/2}. \tag{6}$$

OTB models are generally more appealing than NOTB models since they have less terms to parameterize and their eigenvalue problem can be solved more efficiently. In addition, they present a starting point for linear scaling algorithms such as the recursion methods[31–33] that approximate the exact solution of the electronic structure eigenvalue problem by truncating the density matrix in real space.

III. FROM DFT TO NOTB HAMILTONIANS

A. Projection scheme

Our scheme for deriving bond and overlap integrals for TB models starts from self-consistent plane-wave-based DFT calculations of total energies and electronic structures for a large set of atomic configurations (small molecules, simple crystalline phases) which represent various geometrical arrangements and bonding environments, for instance, sp, sp^2, and sp^3 hybridizations in the case of carbon. Additionally, by varying the bond lengths of molecules or atomic densities of bulk phases we calculate the distance dependence of the interatomic interactions. For each configuration we obtain a set of eigenvalues $\{\varepsilon_i\}$ and eigenfunctions $\{\psi_i\}$ for the occupied states i. Plane-wave DFT calculations have the advantage that all results for the eigenvalues and eigenfunctions can be converged easily with respect to basis set size and that no basis set superposition error is present. This is essential for binary and multicomponent systems.

In the next step we choose a minimal basis of atomic orbitals (AOs) whose shape and range can be varied. The AOs are written as the product of a radial function $f_{\alpha l}(r)$ and a spherical harmonic function $\mathrm{Y}_{lm}(\hat{\mathbf{r}})$ of angular momentum l and m

$$\phi_\mu(\mathbf{r}) = f_{\alpha l}(r)\,\mathrm{Y}_{lm}(\hat{\mathbf{r}}), \quad \mu = (\alpha,l,m). \tag{7}$$

For the parameterized form of the radial AO functions we have tested four different schemes (see next section for a detailed description). The parameterized radial functions of the AOs are optimized to obtain the best AO representation of the DFT wave functions $\{\psi_i\}$ from the plane-wave calculation. This is done by a projection of the $\{\psi_i\}$ onto the minimal AO basis and a minimization of the so-called "spillage" function, which is the amount of electrons lost due to the projection.[26,27]

Since our minimal AO basis is nonorthogonal, it is convenient to introduce first the so-called dual or adjunct basis functions

$$\langle\phi_\mu^+| = \sum_\nu S_{\mu\nu}^{-1}\,\langle\phi_\nu| \tag{8}$$

that are orthogonal to the minimal AO basis

$$\langle\phi_\mu^+|\phi_\nu\rangle = \langle\phi_\mu|\phi_\nu^+\rangle = \delta_{\mu\nu}. \tag{9}$$

With the adjunct basis functions we define the projection operator

$$\widehat{P} = \sum_\mu |\phi_\mu\rangle\langle\phi_\mu^+|. \tag{10}$$

Applying $\widehat{P}$ on $\{\psi_i\}$ gives a measure of how well the DFT wave functions are represented by our minimal AO basis $\{\phi_\mu\}$. Or, in other words, $(\widehat{1}-\widehat{P})|\psi_i\rangle$ describes the part of the DFT wave functions that is lost in the projection. Adding up the norm of the part of the DFT wave functions that is not represented by the minimal AO basis, normalized to the number of electrons N_e in the atomic configuration, gives the electron spillage function[26,27]

$$S_{\mathrm{spill}} = \frac{1}{N_e}\sum_i^{\mathrm{occ}}\langle\psi_i|\widehat{1}-\widehat{P}|\psi_i\rangle. \tag{11}$$

Alternatively, it is also possible to measure how well the band energy is reproduced by the minimal AO basis

$$E_{\mathrm{spill}} = \sum_i^{\mathrm{occ}}(\varepsilon_i - \langle\psi_i|\widehat{P}\widehat{H}\widehat{P}|\psi_i\rangle). \tag{12}$$

Such a projection and optimization scheme has been used previously for reducing multiple-ζ AO basis sets in LCAO calculations[38,39] and for obtaining suitable minimal AO basis set representations of wave functions that allow an analysis of plane-wave DFT calculations in terms of local atomic quantities, such as Mulliken or Löwdin charges, crystal orbital overlap populations, and covalent bond energies.[26,27,40–42]

In the final step, the Hamilton and overlap matrix elements for a given pair of atoms are calculated by using the optimized minimal AO basis together with the self-consistent Hamiltonian of the plane-wave DFT calculation. The fundamental Slater-Koster bond and overlap integrals are then extracted simply by rotating the matrices into a bond-oriented coordinate system. Since the full self-consistent Hamiltonian of the reference configuration is applied, the Hamilton matrix elements contain contributions from three-center integrals. Consequently, the derived π and δ bond integrals vary with the orientation of the atomic orbitals perpendicular to the bond axis, and all bond integrals depend on the choice of the reference configuration (though both dependencies are weak, as will be shown in the next sections). To arrive at unique two-center Slater-Koster bond integrals that only depend on interatomic distance, we compute the π and δ bond integrals by taking rotational averages, and the final Slater-Koster bond integrals are determined by averaging the results from our representative set of reference configurations. With this procedure the ambiguity due to the three-center terms is removed, while at the same time their effect is included "on

average" in the Slater-Koster integrals. In addition, with our projection scheme also the dependence of the on-site matrix elements on the local atomic environment is automatically extracted.

The whole projection procedure has been implemented in our mixed-basis pseudopotential DFT code.[43,44] All expressions are calculated in reciprocal space using Fourier transformations[26,27] so that the radial functions of the atomic orbitals may have arbitrary shapes and ranges. A suite of scripts allows to derive the complete set of distance-dependent bond and overlap integrals for an element or a binary compound within a short period of time (typically a few hours) and in a fully automated manner.

B. Optimization of the minimal basis

For the optimization of the minimal atomic orbital basis we tested four different parameterized forms of the radial AO functions $f_{\alpha l}(r)$. In all four cases self-consistent solutions of the DFT equations for isolated, spherical atoms serve as the starting point for the construction of flexible parameterized representations of the $f_{\alpha l}(r)$ functions. The DFT equations are solved on a radial grid with or without using a confinement potential. Specifically, the four implemented choices for the radial AO functions $f_{\alpha l}(r)$ are as follows.

(A) The radial functions $f_{\alpha l}^{\rm at}(r)$ of the nonconfined free atom are contracted and multiplied by a smooth cutoff function[45]

$$f_{\alpha l}(r) = f_{\alpha l}^{\rm at}(\lambda_{\alpha l}\, r)\left(1 - e^{-\gamma_{\alpha l}(R_{\alpha l}^{\rm cut} - r)^2}\right). \qquad (13)$$

In the projection procedure the contraction factors $\lambda_{\alpha l}$, the cutoff radii $R_{\alpha l}^{\rm cut}$, and the widths $\gamma_{\alpha l}$ of the cutoff functions are optimized simultaneously for all atomic orbitals to minimize the spillage function $S_{\rm spill}$.

(B) The solutions of the radial Schrödinger equation for the isolated atom in a confinement potential are taken as radial functions $f_{\alpha l}(r)$, while optimizing the shape, onset, and range of the confinement potential. For the confinement potential we have taken the following analytic form:

$$v_{\alpha l}^{\rm conf}(r) = \left(\frac{r - R_{\alpha l}^0}{R_{\alpha l}^{\rm cut} - R_{\alpha l}^0}\right)^2 \frac{A_{\alpha l}(A_{\alpha l} - 1)}{\left(R_{\alpha l}^{\rm cut} - r\right)^2} \qquad (14)$$

with $R_{\alpha l}^0 \leqslant r \leqslant R_{\alpha l}^{\rm cut}$. The confinement potential is zero for $0 \leqslant r \leqslant R_{\alpha l}^0$. The variable parameters for minimizing the spillage function are the coefficients $A_{\alpha l}$, the onset radii $R_{\alpha l}^0$, and the range $R_{\alpha l}^{\rm cut}$ of the confinement potential. Typical confinement potentials are shown in Fig. 1(a). The analytic form of Eq. (14) has several advantages compared to previous choices of confinement potentials.[12,46–53] First, the atomic wave functions of the free atoms, which are very well adapted to the external potential in the ionic core regions of the atoms, remain unchanged inside a sphere with radius $R_{\alpha l}^0$. The quadratic onset of the confinement potential guarantees that the derivatives of the wave functions remain continuous up to the third order. Second, the pole in the potential $v_{\alpha l}^{\rm conf}$ ensures that the atomic orbitals are localized and become zero outside the radius $R_{\alpha l}^{\rm cut}$. Third, by using a quadratic pole at $R_{\alpha l}^{\rm cut}$ the radial functions $f_{\alpha l}(r)$ decay as $(R_{\alpha l}^{\rm cut} - r)^{A_{\alpha l}}$, as can be shown by a Taylor expansion. Therefore, the smoothness of the decay of the radial functions can be controlled in a simple way by setting a lower limit for the allowed range for $A_{\alpha l}$ in the optimization procedure.

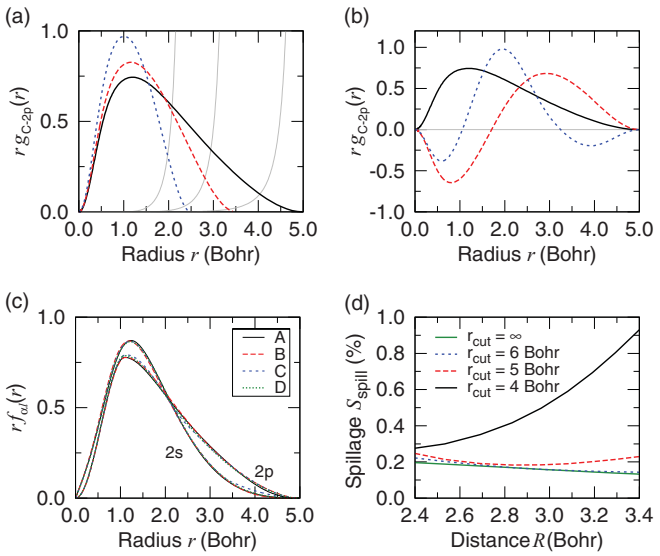

FIG. 1. (Color online) (a) Triple-ζ basis functions $g_{\alpha l}^{(k)}(r)$ for carbon $2p$ as obtained from DFT calculations for the free C atom in confinement potentials with different cutoff radii. The three basis functions are used to optimize the carbon $2p$ radial AO function according to scheme (C). The confinement potentials are shown by thin gray lines. (b) $2p$ radial function for carbon (solid line) from a DFT calculation for the free C atom in a confinement potential with $R_{\alpha l}^{\rm cut} = 5$ Bohr, together with the first two derivatives with respect to the occupation numbers (dashed lines). The three functions were used as basis functions $g_{\alpha l}^{(k)}(r)$ to optimize the carbon $2p$ radial AO function according to scheme (D). (c) Optimized $2s$ and $2p$ radial AO functions according to schemes (A)–(D) for diamond at the equilibrium volume. (d) Electron spillage function $S_{\rm spill}$ as a function of the C–C distance R between nearest-neighbor atoms in diamond. The radial AO functions were optimized using scheme (A) while keeping the range $R_{\alpha l}^{\rm cut}$ fixed at the value given in the inset.

(C) The atomic radial functions $f_{\alpha l}(r)$ are represented by linear combinations of basis functions $g_{\alpha l}^{(k)}(r)$ with different ranges. Our experience is that three basis functions are usually sufficient to get well-converged results ("triple-ζ basis"):

$$f_{\alpha l}(r) = g_{\alpha l}^{(0)}(\lambda_{\alpha l}\, r) + c_{\alpha l}^{(1)}\, g_{\alpha l}^{(1)}(\lambda_{\alpha l}\, r) + c_{\alpha l}^{(2)}\, g_{\alpha l}^{(2)}(\lambda_{\alpha l}\, r). \qquad (15)$$

Optimization parameters are the contraction factors $\lambda_{\alpha l}$ and the linear coefficients $c_{\alpha l}^{(1)}$ and $c_{\alpha l}^{(2)}$. In principle, any scheme that is useful for finding suitable localized atom-centered basis sets for electronic structure calculations might be employed to generate a set of $g_{\alpha l}^{(k)}(r)$ functions.[47–57] Specifically, we have taken the $g_{\alpha l}^{(k)}(r)$ from DFT calculations for free atoms in the confinement potential of Eq. (14) with fixed values for $R_{\alpha l}^0$ and $A_{\alpha l}$. $R_{\alpha l}^{\rm cut}$ controls the extent of the basis functions. Several different schemes have been proposed in the literature on how to choose the range of the $g_{\alpha l}^{(k)}(r)$ functions.[39,50–53] All of them are closely related to the "split valence" scheme of quantum chemistry.[54] In the present work, the cutoff radii $R_{\alpha l}^{\rm cut}$ were chosen in such a way that the confinement potential increased the energy eigenvalue of the corresponding atomic orbital in steps of 0.4 Ry (Refs. 39 and 50). The onset of the confinement

potential was set to 40% of the cutoff radius and $A_{\alpha l}$ was taken to be 2. A set of three $g_{\alpha l}^{(k)}(r)$ basis function for the carbon $2p$ orbital, which was generated by this procedure, is shown in Fig. 1(a). A similar scheme was used recently by Madsen *et al.*[39] to determine a TB parameterization for Fe by downfolding the results of triple-ζ LCAO calculations to a minimal basis representation.

(D) As in scheme (C) the atomic radial functions $f_{\alpha l}(r)$ are represented by linear combinations of three basis functions $g_{\alpha l}^{(k)}(r)$. For the basis functions $g_{\alpha l}^{(k)}(r)$ we take the radial function from a DFT calculation for the free atom in the confinement potential of Eq. (14) with fixed parameters together with the first two derivatives of the radial function with respect to the occupation numbers of the atomic orbitals.[55–57] The derivatives are determined by repeating the DFT calculation for the free atom in its confinement potential for slightly ionic configurations (typically we remove 0.1 and 0.2 electrons) and then taking first- and second-order finite differences. The derivatives of the radial functions with respect to the occupation numbers are closely related to the energy eigenvalue derivatives in the so-called "linear methods," [e.g., the linear muffin-tin orbital (LMTO) and the linear augmented plane-wave (LAPW) methods].[16,56,58] The three basis functions $g_{\alpha l}^{(k)}(r)$ are automatically pairwise orthogonal and exhibit an increasing number of nodes. Fig. 1(b) shows a set of representative $g_{\alpha l}^{(k)}(r)$ functions for the carbon $2p$ orbital.

All four schemes were thoroughly tested. We found that they all work equally well, giving spillage values of about 10^{-2} per electron. The example of the carbon $2s$ and $2p$ orbitals in Fig. 1(c), optimized for the diamond structure at the equilibrium volume, shows that the differences in the optimized radial functions are rather small. From a practical point of view, the schemes (A) and (D) are most convenient since they are numerically most stable and thus allow for a full automatization of the projection and the derivation of the bond and overlap integrals.

The final point requiring some further consideration is the range of the atomic orbitals in the optimized minimal basis set. The range of the radial functions $f_{\alpha l}(r)$ is a variational parameter only in the schemes (A) and (B), whereas in the schemes (C) and (D) it is mostly determined by the choice of the cutoff radius for the confinement potential (only small variation via the contraction factor $\lambda_{\alpha l}$ is possible). From our investigations it appears that the results are rather insensitive to the choice of $R_{\alpha l}^{\rm cut}$. In Fig. 1(d) we plotted the electron spillage $S_{\rm spill}$ for diamond at different volumes after optimizing the minimal AO basis using scheme (A) but keeping $R_{\alpha l}^{\rm cut}$ fixed. As long as the AO radial functions are not too short-ranged, the spillage values are very similar. Only if $R_{\alpha l}^{\rm cut}$ becomes too small, the spillage starts to increase significantly. Typically, this onset of the increase in the spillage is a convenient choice for the range of the radial functions in the minimal atomic orbital basis set.

C. Application to carbon

In this section we illustrate our projection procedure for the derivation of TB parameters for carbon. The first step is to choose a set of reference configurations from which the bond and overlap integrals are obtained. Since we are interested in the derivation of universal and transferable TB parameters, this set should represent a broad range of structures and bonding configurations. To fulfill this criterion, our choice comprises several hydrocarbon molecules (ethane, ethylene, acetylene), the infinite linear chain of carbon atoms, the planar structure of graphene, and the bulk diamond phase. This set thus encompasses the most relevant atomic coordinations (one- to four-fold in one to three dimensions) and hybridizations (sp, sp^2, and sp^3) of carbon atoms. The distance dependence of the Slater-Koster integrals is then monitored by changing uniformly the bond length in molecules or the lattice constant of bulk structures by ± 10 % and by calculating the bond and overlap integrals for first, second, and third nearest-neighbor atom pairs.

In the second step, DFT calculations and subsequent projection procedures are carried out for all configurations. Apart from the chosen projection scheme, the resulting spillage depends on whether the radial AO functions are optimized for each individual configuration or not. Figure 2(a) shows the electron spillage as a function of C–C bond distance R for two different choices of how the optimization of the AOs is done. As expected, the lowest spillage values are achieved when the radial functions of the minimal atomic orbital basis are re-optimized for every structure (dashed lines). Since the re-optimization of the radial AO functions is rather time consuming, we also tested the performance of a fixed AO basis that is only optimized for a limited set of structures. Indeed, we find that the individual re-optimizations are not necessary. As shown by the solid lines in Fig. 2(a), the overall spillage remains almost equally low when the radial AO functions are optimized only once by a simultaneous minimization of the combined electron spillage for the equilibrium geometries of the linear carbon chain, graphene, and diamond (i.e., three atomic configurations). Even more important, with this fixed optimum AO basis also the spillage in the electronic band energy remains at the same low level as for the individually re-optimized basis [see Fig. 2(b)].

Since the single optimum AO basis can reliably describe the bonding in all reference structures, we have only used this

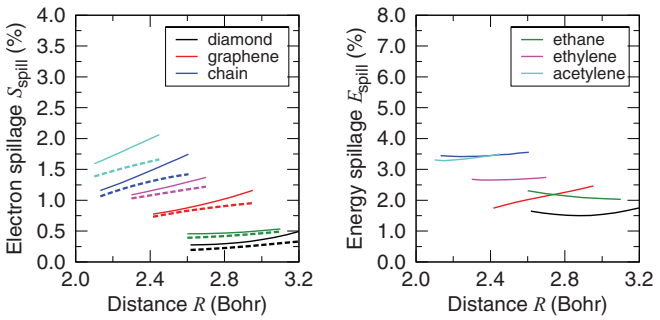

FIG. 2. (Color online) Electron spillage $S_{\rm spill}$ (left) and energy spillage $E_{\rm spill}$ (right, given in percent of the DFT result) as a function of the C–C distance R between nearest-neighbor atoms in different carbon containing structures. Dashed lines: the radial AO functions were optimized for all structures and C–C distances using scheme (D); solid lines: a fixed AO basis was used which was obtained by optimizing the AO radial functions simultaneously for the linear carbon chain, graphene, and diamond at their equilibrium geometries using scheme (D).

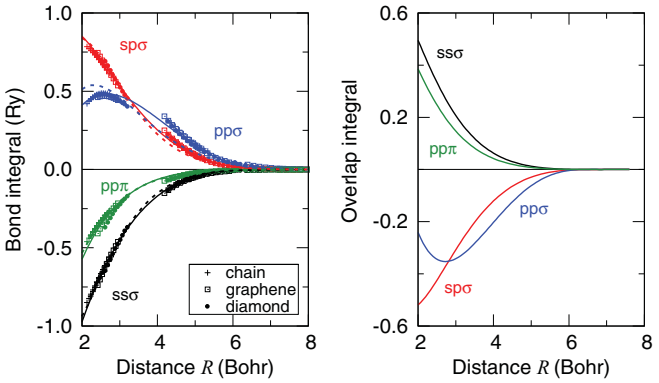

FIG. 3. (Color online) Slater-Koster NOTB bond (left) and overlap (right) integrals for carbon calculated with the fixed AO basis which was obtained by optimizing the AO radial functions simultaneously for the linear carbon chain, graphene, and diamond at their equilibrium geometry using scheme (D). Symbols: results from the projection for different carbon containing structures; solid lines: interpolation through the data points using an exponential function times a third-order polynomial; dotted lines: projection result for the carbon dimer.

fixed AO basis for completing the final step, the calculation of the Slater-Koster bond and overlap integrals. The resulting distance dependencies of these integrals are shown in Fig. 3. The convenient advantage of a fixed AO basis is that there is no scatter in the overlap integrals, and they are therefore plotted as continuous lines in Fig. 3. On the other hand, since the bond integrals contain contributions from three-center integrals, they might vary strongly according to the bonding environment and their description by simple distance-dependent functions is sometimes problematic.[22,23] However, the results shown in the left panel of Fig. 3 demonstrate that the carbon bond integrals obtained using our projection scheme exhibit a very good transferability between the chain, graphene, and diamond: They can be represented well by smooth functions of interatomic distance only. The full lines in Fig. 3 are obtained by fitting a simple exponential function times a third-order polynomial to the projection data. Only for the $pp\pi$ integrals some small scatter is visible for the first nearest neighbor.

The importance of including the three-center contributions to the bond integrals in an averaged way can be seen by comparing the full and dashed lines in the left panel of Fig. 3. The dashed lines correspond to the carbon dimer where no three-center contributions are present. Relatively large three-center contributions are seen for the $pp\sigma$ integrals, which effectively extend the range of these integrals.

In Fig. 4 we present a comparison of calculated band structures for graphene and diamond. The plots demonstrate that the DFT results (thick gray lines) for both structures are reproduced very well by the NOTB Hamiltonian with bond and overlap integrals from our projection procedure (solid red lines). When the interpolated bond integrals (i.e., the solid lines in Fig. 3) are used instead of the projected values, the occupied valence bands remain basically unchanged. The overall agreement of both TB band structures with the DFT result is significantly better than for the case when bond integrals are calculated from unoptimized AO functions (blue dotted lines) as in the DFTB approach.

The calculation of total energies in a TB scheme requires also a parameterization of the repulsive energy term in Eq. (1). In its simplest form, this energy term may be written as the sum of pair potentials,[6,35] but often more elaborate functional forms are chosen which utilize additional embedding functions or many body terms.[17,18,39,59–62] The description of repulsive interactions cannot be derived directly from DFT calculations in a similar way as our bond and overlap integrals. Instead, the chosen functional forms need to be parameterized by fitting to forces or total energies of representative atomic configurations.

To demonstrate that such an approach also works in conjunction with the bond and overlap integrals derived using our projection scheme, we constructed a simple NOTB total energy model for carbon. A pair potential ansatz was chosen for the description of the repulsion with the potential function $\Phi(R)$ represented by an exponential times a polynomial (the same functional form as for our bond and overlap integrals). The decay constant of the exponential and the coefficients of the polynomial were fitted to reproduce the total energies of the most relevant carbon phases. As shown in Fig. 5, this basic ansatz already provides a very reasonable representation of the total energies for the linear carbon chain, graphene, and diamond that are comparably good as those of previous

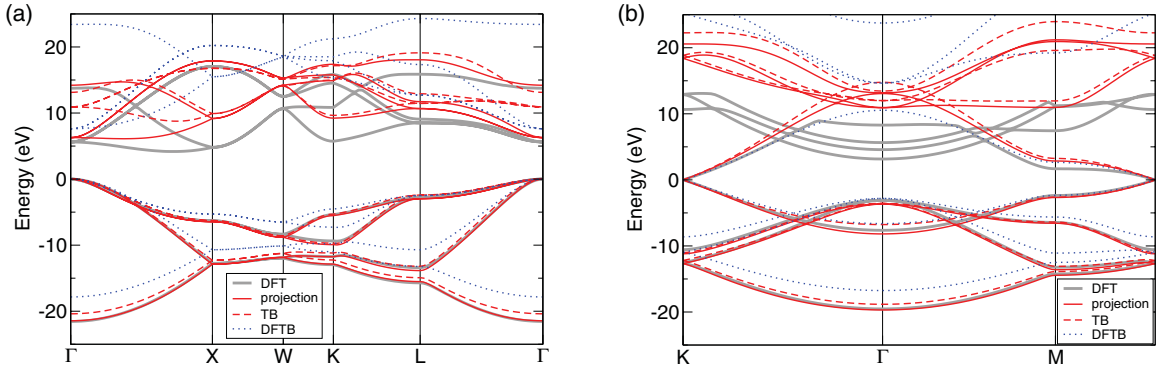

FIG. 4. (Color online) Band structure for (a) diamond and (b) graphene. Gray lines: mixed-basis DFT result; red solid lines: NOTB band structure with Slater-Koster bond and overlap integrals from the projection procedure; red dashed lines: NOTB band structure from interpolated Slater-Koster bond and overlap integrals (see solid lines in Fig. 3); blue dotted lines: DFTB band structure.[12] The Fermi level/valence band maximum is set to 0 eV.

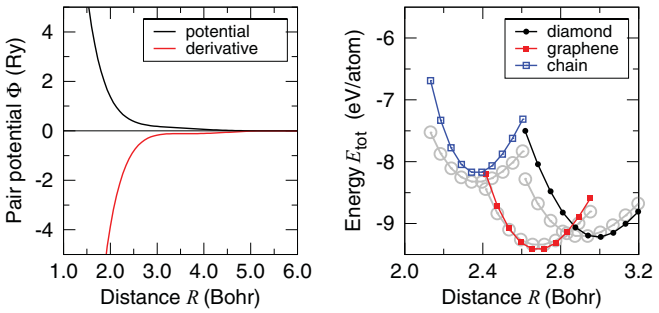

FIG. 5. (Color online) Left: Carbon pair potential $\Phi(R)$ and its first derivative. Right: Binding energy of the linear carbon chain, graphene, and diamond as function of the nearest-neighbor C–C distance R. Gray: mixed-basis DFT result; red: NOTB calculation.

models.[12,59,63] It should be noted that this model is preliminary and there is still much potential for further optimization. Our ongoing studies of highly distorted bonding environments (e.g., amorphous structures) indicate that a more sophisticated description of the repulsive interactions might be needed, which will be the focus of future work.

D. Application to Ti and TiC

In addition to carbon, we applied our projection scheme to a series of transition metals (Ti, Zr, Nb, Ta, Mo, W, Fe) (Refs. 64 and 65) as well as to several binary systems (Si-C, Ti-C, Si-N, Ti-N) (Refs. 62 and 65) to test extensively its applicability to various bonding environments. Here we present the results for Ti as a representative transition metal and demonstrate the transferability of the optimized basis for binary TiC.

The NOTB ss, sd, and dd bond and overlap integrals for Ti obtained from the projection are displayed as functions of interatomic distance in Fig. 6. In these calculations, the spd AO basis was first optimized for the hexagonal close-packed (hcp) phase of Ti at its equilibrium volume and then used without further modification for projections in other bulk phases at different volumes. As in the case of carbon, with the fixed basis the overlap integrals are simple continuous functions of the interatomic distance only and do not vary for different crystal structures (see top panels of Fig. 6). On the other hand, the bond integrals show some variations among different structures (see bottom panels of Fig. 6). The scatter is, however, much smaller than in results obtained using the QUAMBO approach.[23] Especially the dd bond integrals can be well approximated by simple continuous functions. The weaker dependence on the environment is most likely related to the fixed AO basis in our approach and also its relatively short range. The QUAMBOs need to be newly constructed for every bonding environment and the requirement to reproduce all occupied electronic states makes them significantly longer ranged.

Figure 7 shows a comparison of DFT and projected band structures for three distinct bulk phases of Ti. The band structure plots in Fig. 7 again demonstrate that the orbitals optimized just for the equilibrium hcp phase provide also an excellent description of the electronic structure of other phases with very different bonding environments. Additionally, Fig. 8 shows that this transferability is not limited to elemental phases, but that the optimized atomic orbitals obtained for the two elements can even capture the bonding in binary compounds, namely two distinct phases of TiC, without any re-optimization. This is a very encouraging result since it demonstrates a possibility to construct transferable TB models for multicomponent systems without a need for extensive fitting.

IV. FROM NOTB TO OTB HAMILTONIANS

The atomic orbitals used in our projection scheme are orthogonal when they are centered on the same atom but nonorthogonal for centers at different atomic sites. However, as already mentioned above, orthogonal TB models are simpler and therefore more appealing than nonorthogonal ones. In addition, the OTB schemes serve as a basis for approximate linear-scaling schemes such as the bond-order potentials.[31–33] In this last section, we therefore address two issues associated

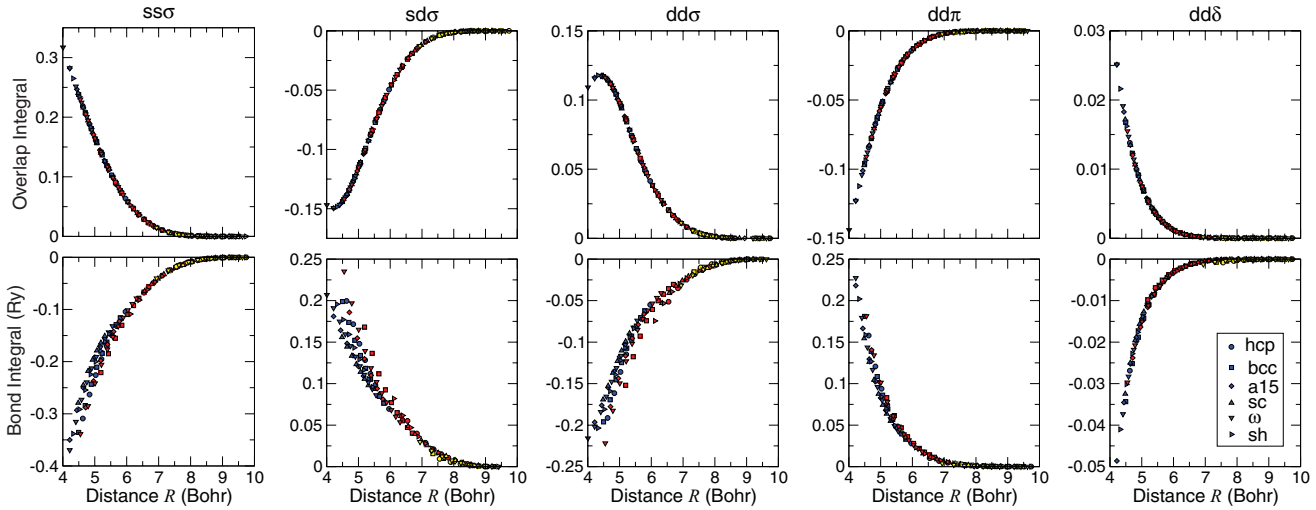

FIG. 6. (Color online) Slater-Koster NOTB bond and overlap integrals for Ti obtained by applying our projection scheme to a series of crystal structures at different volumes.

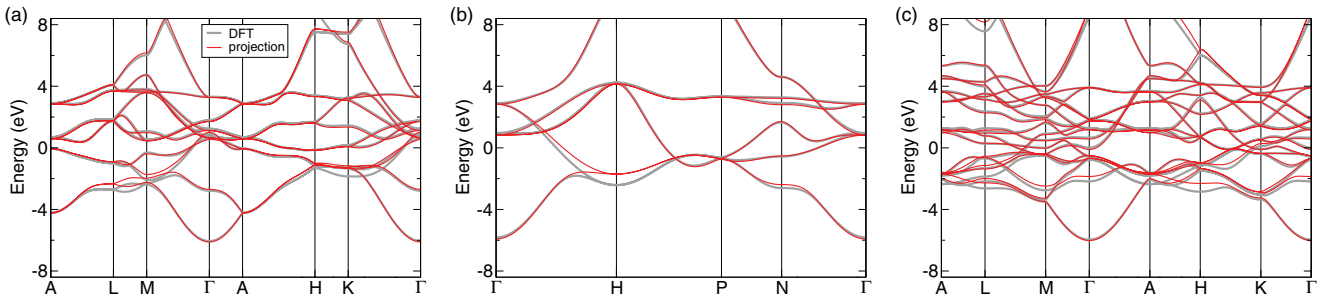

FIG. 7. (Color online) Band structures of bulk Ti in the (a) hcp, (b) bcc, and (c) ω phase. Gray lines: mixed-basis DFT result; red solid lines: NOTB result with Slater-Koster bond and overlap integrals from the projection procedure. The Fermi level is at 0 eV.

with the derivation of the simplest possible OTB models—the orthogonalization and the basis reduction.

A. Löwdin transformation and basis reduction

The orthogonalization of the AO basis is, in principle, a straightforward mathematical procedure, but it is not a unique one. The most natural and convenient transformation for derivation of OTB models is Löwdin's symmetrical orthogonalization.[37] Its main advantages are that it produces orthogonal functions that have the same symmetry as the original nonorthogonal ones and that these functions are least distorted in the least-square sense.[66] However, as every orthogonalization, the Löwdin orthogonalization is environment dependent (i.e., the magnitudes, ranges, and distance dependences of the resulting OTB bond integrals depend not only on the NOTB Hamilton and overlap matrix elements but also on the geometry of the particular atomic configuration). It is therefore necessary to obtain a thorough insight into the NOTB-OTB relationship, particularly in terms of the transferability of the bond integrals.

Additionally, it is often possible to reduce the minimal spd AO basis even further and to retain only orbitals that contribute most to the chemical bonding. This reduction results in the simplest possible TB models that are still able to capture the key essence of chemical bonding while being computationally most efficient. The basis reduction can be exemplified on the case of middle transition metals with partially filled d bands. The cohesion in these elements is primarily governed by d electrons, so that the s and p orbital interactions do not need to be treated explicitly and their effective contributions to the binding energy can be incorporated, for instance, via pair or simple many-body terms.[19,39] Similarly, for transition-metal compounds, such as TiC, it is possible to a good approximation to consider only a Ti(d)–C(p) OTB model.[62] However, in this case the reduction of the basis has its limitations. While the simplest Ti(d)–C(p) model is likely to be sufficient for the description of the binary system alone, for studies of TiC/C interfaces a more complete sp basis on C has to be retained to ensure a proper transferability between the elemental carbon and the TiC compound. The issue is therefore rather subtle and depends also on the particular problem. The advantage of our projection scheme is that we can study in detail the influence of a reduced basis on the electronic properties in a well-controlled way.

The last issue that needs to be considered when obtaining the reduced OTB parameters is whether the orthogonalization is done either before or after the basis reduction. In simple terms, the orthogonal orbitals are mixtures (linear combinations) of the original orbitals with orbitals located on the neighboring atoms. If the full spd basis is kept, the orthogonal orbitals are admixtures of all three orbital types and consequently the OTB Hamiltonian elements are more affected by their surroundings; if the basis is reduced before orthogonalization, the environment dependence of the resulting Hamiltonian elements is weaker. The physical meaning of the orthogonalization can be also understood within the concept of bond screening.[60,67] Nguyen-Manh *et al.*[17] showed

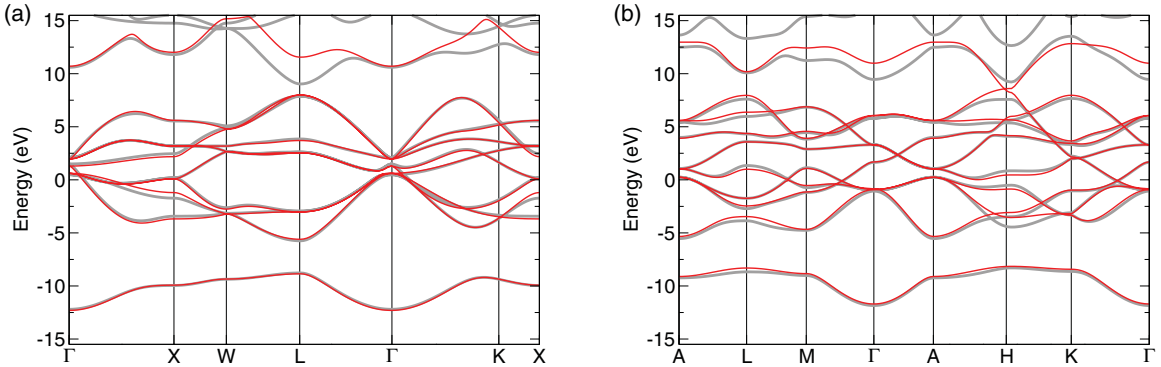

FIG. 8. (Color online) Band structures of bulk TiC in the (a) sodium chloride (B1) and (b) tungsten carbide (B_h) phase. Gray lines: mixed-basis DFT result; red solid lines: NOTB result with Slater-Koster bond and overlap integrals from the projection procedure. The Fermi level is at 0 eV.

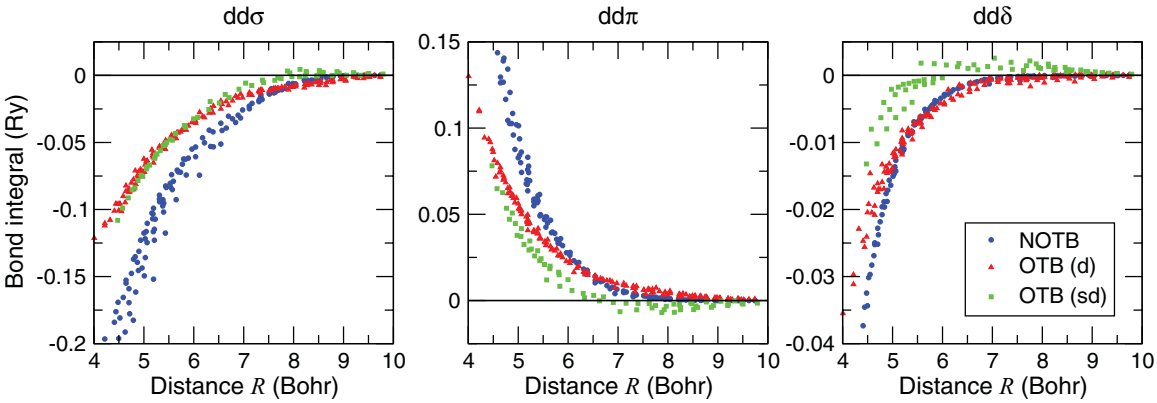

FIG. 9. (Color online) Comparison of NOTB, d-OTB, and sd-OTB bond integrals for Ti obtained by applying our projection scheme to a number of crystal structures at different volumes.

that the environmental dependence of OTB parameters can be derived from the NOTB theory in the form of an analytical screening function. The screening function represents the fact that a given bond is influenced by the presence of other atoms in its vicinity. The strength of the screening is proportional to the overlap with orbitals on the neighboring atoms. The issue of doing orthogonalization before or after basis reduction is exemplified for Ti in the following section.

B. OTB models for Ti

Our investigations for transition metals confirm the effect of basis reduction on the behavior of OTB parameters. Figure 9 gives a comparison of the original NOTB dd bond integrals for Ti from Fig. 6 with corresponding orthogonalized ones obtained using a completely reduced d-only and partly reduced sd basis. In both cases, the orthogonalization leads to smaller absolute values of the bond integrals and it increases the range of the interactions. This increase is, however, not dramatic, showing that the orthogonalization does not necessarily lead to long-range interactions.

Another finding is that the orthogonalization does not cause an overall decrease of the transferability of the bond integrals. In fact, the orthogonal $dd\sigma$ bond integrals turn out to be more transferable than the NOTB ones. When the completely reduced d-only basis is used, the environment dependence of all three $dd\sigma$, $dd\pi$, and $dd\delta$ orthogonal bond integrals is very weak. They can be described very well by simple continuous functions, which depend on the interatomic distance only. For the partly reduced sd basis the screening effects of the s orbitals are visible on the $dd\pi$ and $dd\delta$ bond integrals. In this case, the s orbitals contribute significantly to the screening of the interatomic bonds and cause stronger environmental effects with some of the values corresponding to more distant neighbors even changing the sign. The more complete basis therefore leads, as expected, to bond integrals that are environment dependent.

As a validation of the d-only OTB model, we show in Fig. 10 again a comparison of DFT and OTB band structures for three bulk phases of Ti (cf., Fig. 7). Obviously, since the s orbitals are not present, the corresponding lowest bands are missing, but the d band is reproduced well, especially for the hcp and bcc phases. In the ω phase, a rather strong pd hybridization occurs, which pushes some of the unoccupied d bands up. Since this effect is also missing in the d-only model, the band structure above the Fermi level is reproduced less satisfactorily for this phase, and the width of the d band is somewhat underestimated.

V. SUMMARY AND CONCLUSION

In this work, a rigorous bottom-up approach is presented for deriving TB Hamiltonians from first-principles DFT calculations without the need for empirical fitting to materials data. The approach is universally applicable to both elements and compounds in arbitrary structural and chemical arrangements.

The procedure from DFT to NOTB models is built on the projection of DFT wave functions on basis sets of atomic-

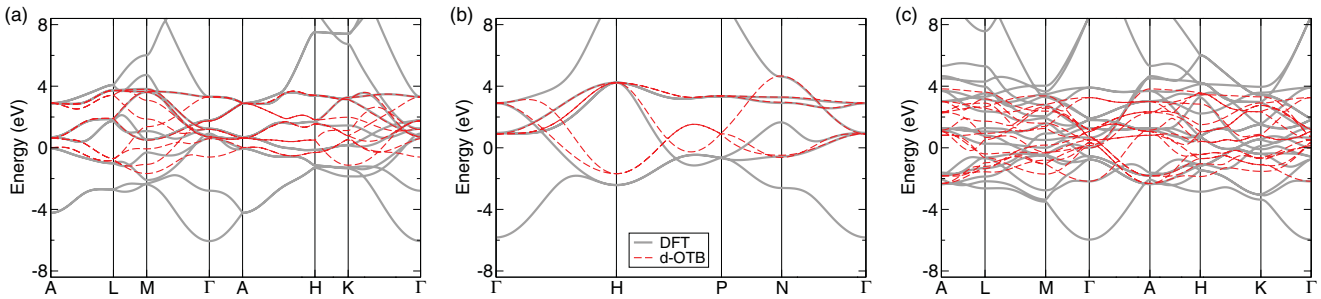

FIG. 10. (Color online) Band structures of bulk Ti in the (a) hcp, (b) bcc, and (c) ω phase. Gray lines: mixed-basis DFT result; red dashed lines: d-OTB result. The Fermi level is at 0 eV.

orbital-like functions, which are strictly angular-momentum eigenfunctions and whose radial ranges and shapes are optimized with respect to completeness of the projection (minimum spillage). As illustrated by the comparison of DFT and NOTB band structures for several crystalline phases of the elements C and Ti and their compound TiC, nonorthogonal TB bond integrals are obtained which are well transferable to various molecular and crystalline configurations. Their distance dependencies are short ranged and can be well represented by smooth analytical functions. Their environment dependencies are rather weak and can be well controlled.

The procedure from NOTB to OTB models involves two distinct steps, the mathematical orthogonalization and the physical reduction of the basis set. As illustrated for the case of Ti, the sequential order of orthogonalization and reduction is important and can be advantageous for getting best suited orthogonal TB Hamiltonians for specific purposes. Namely for Ti and other middle transition metals whose bonding and structure are mainly governed by partially filled d bands, the reduction of the optimized spd-NOTB basis to only the d-AOs before the orthogonalization leads to a d-OTB model whose bond integrals have rather short ranges and negligible environment dependences. The comparison of DFT and d-OTB band structures for different crystalline phases of Ti demonstrates the good transferability of the d-OTB model as well. Furthermore, our methodology simplifies the development of total-energy TB models and closely related bond-order potentials that include a parameterization of the repulsive energy term. Such models have been recently developed for Fe (Ref. 64) as well as the binary systems Ti-C and Ti-N (Ref. 62) and applied in atomistic simulations of complex crystalline defects.

Altogether, our presented bottom-up approach founded on first-principles DFT calculations has the potential to cope with the whole spectrum of materials modeling from accurate semi-empirical NOTB electronic-structure calculations via reduced OTB models to linear-scaling atomistic BOP simulations for both single-component and multi-component materials.

ACKNOWLEDGMENTS

The authors acknowledge the collaboration and many fruitful discussions with Ralf Drautz, Georg Madsen, Elena Roxana Margine, Aleksey Kolmogorov, Paul Kamensky, Jan Gehrmann, and David Pettifor. A. U. thanks the Fonds der Chemischen Industrie (FCI) for a Kekulé Fellowship. Financial support was provided by the German Research Foundation (DFG) via Grants No. MR 22/5-1 and No. ME 2670/3-1, by the German Ministry of Education and Research (BMBF), Grant No. 03X0511, and by the European Comission through Contract No. NMP.2010.2.5-1.263335 (MultiHy).

*bernd.meyer@chemie.uni-erlangen.de

[1] R. M. Martin, *Electronic Structure: Basic Theory and Practical Methods* (Cambridge University Press, Cambridge, England, 2004).
[2] M. W. Finnis and J. E. Sinclair, Philos. Mag. A **50**, 45 (1984).
[3] F. H. Stillinger and T. A. Weber, Phys. Rev. B **31**, 5262 (1985); **33**, 1451(E) (1986).
[4] J. Tersoff, Phys. Rev. Lett. **56**, 632 (1986).
[5] D. W. Brenner, Phys. Rev. B **42**, 9458 (1990).
[6] M. W. Finnis, *Interatomic Forces in Condensed Matter* (Oxford University Press, New York, 2003).
[7] J. C. Slater and G. F. Koster, Phys. Rev. **94**, 1498 (1954).
[8] C. M. Goringe, D. R. Bowler, and E. Hernandez, Rep. Prog. Phys. **60**, 1447 (1997).
[9] A. P. Horsfield and A. M. Bratkovsky, J. Phys. Condens. Matter **12**, R1 (2000).
[10] D. A. Papaconstantopoulos and M. J. Mehl, J. Phys. Condens. Matter **15**, R413 (2003).
[11] H. Amara, C. Bichara, and F. Ducastelle, Phys. Rev. B **73**, 113404 (2006).
[12] D. Porezag, Th. Frauenheim, Th. Köhler, G. Seifert, and R. Kaschner, Phys. Rev. B **51**, 12947 (1995).
[13] M. Elstner, D. Porezag, G. Jungnickel, J. Elsner, M. Haugk, Th. Frauenheim, S. Suhai, and G. Seifert, Phys. Rev. B **58**, 7260 (1998).
[14] G. Seifert, J. Phys. Chem. A **111**, 5609 (2007).
[15] P. Koskinen and V. Mäkinen, Comput. Mater. Sci. **47**, 237 (2009).
[16] O. K. Andersen and O. Jepsen, Phys. Rev. Lett. **53**, 2571 (1984).
[17] D. Nguyen-Manh, D. G. Pettifor, and V. Vitek, Phys. Rev. Lett. **85**, 4136 (2000).
[18] M. Mrovec, D. Nguyen-Manh, D. G. Pettifor, and V. Vitek, Phys. Rev. B **69**, 094115 (2004).
[19] M. Mrovec, R. Gröger, A. G. Bailey, D. Nguyen-Manh, C. Elsässer, and V. Vitek, Phys. Rev. B **75**, 104119 (2007).
[20] W. C. Lu, C. Z. Wang, M. W. Schmidt, L. Bytautas, K. M. Ho, and K. Ruedenberg, J. Chem. Phys. **120**, 2629 (2004).
[21] W. C. Lu, C. Z. Wang, T. L. Chan, K. Ruedenberg, and K. M. Ho, Phys. Rev. B **70**, 041101(R) (2004).
[22] W. C. Lu, C. Z. Wang, K. Ruedenberg, and K. M. Ho, Phys. Rev. B **72**, 205123 (2005).
[23] T.-L. Chan, Y. X. Yao, C. Z. Wang, W. C. Lu, J. Li, X. F. Qian, S. Yip, and K. M. Ho, Phys. Rev. B **76**, 205119 (2007).
[24] X. Qian, J. Li, L. Qi, C.-Z. Wang, T.-L. Chan, Y.-X. Yao, K.-M. Ho, and S. Yip, Phys. Rev. B **78**, 245112 (2008).
[25] Y. X. Yao, C. Z. Wang, G. P. Zhang, M. Ji, and K.-M. Ho, J. Phys. Condens. Matter **21**, 235501 (2009).
[26] D. Sánchez-Portal, E. Artacho, and J. M. Soler, Solid State Commun. **95**, 685 (1995).
[27] D. Sánchez-Portal, E. Artacho, and J. M. Soler, J. Phys. Condens. Matter **8**, 3859 (1996).
[28] X.-P. Li, R. W. Nunes, and D. Vanderbilt, Phys. Rev. B **47**, 10891 (1993).
[29] R. W. Nunes and D. Vanderbilt, Phys. Rev. B **50**, 17611 (1994).
[30] S. Goedecker, Rev. Mod. Phys. **71**, 1085 (1999).
[31] D. G. Pettifor, Phys. Rev. Lett. **63**, 2480 (1989).
[32] A. P. Horsfield, A. M. Bratkovsky, D. G. Pettifor, and M. Aoki, Phys. Rev. B **53**, 1656 (1996).
[33] For a collection of review papers on BOPs see special issue of Prog. Mater. Sci. **52** (2007), edited by M. W. Finnis and R. Drautz.

[34]J. Harris, Phys. Rev. B **31**, 1770 (1985).
[35]A. P. Sutton, M. W. Finnis, D. G. Pettifor, and Y. Ohta, J. Phys. C **21**, 35 (1988).
[36]W. M. C. Foulkes and R. Haydock, Phys. Rev. B **39**, 12520 (1989).
[37]P.-O. Löwdin, J. Chem. Phys. **18**, 365 (1950).
[38]E. Francisco, L. Seijo, and L. Pueyo, J. Solid State Chem. **63**, 391 (1986).
[39]G. K. H. Madsen, E. J. McEniry, and R. Drautz, Phys. Rev. B **83**, 184119 (2011).
[40]M. D. Segall, C. J. Pickard, R. Shah, and M. C. Payne, Mol. Phys. **89**, 571 (1996).
[41]N. Börnsen, B. Meyer, O. Grother, and M. Fähnle, J. Phys. Condens. Matter **11**, L287 (1999).
[42]S. Köstlmeier, C. Elsässer, and B. Meyer, Ultramicroscopy **80**, 145 (1999).
[43]B. Meyer, F. Lechermann, C. Elsässer, and M. Fähnle, FORTRAN 90 program for mixed-basis pseudopotential calculations for crystals, Max-Planck-Institut für Metallforschung, Stuttgart.
[44]B. Meyer, Ph.D. thesis, Universität Stuttgart, 1998.
[45]C. Elsässer, N. Takeuchi, K. M. Ho, C. T. Chan, P. Braun, and M. Fähnle, J. Phys. Condens. Matter **2**, 4371 (1990).
[46]O. F. Sankey and D. J. Niklewski, Phys. Rev. B **40**, 3979 (1989).
[47]P. D. Haynes and M. C. Payne, Comput. Phys. Commun. **102**, 17 (1997).
[48]A. P. Horsfield, Phys. Rev. B **56**, 6594 (1997).
[49]S. D. Kenny, A. P. Horsfield, and H. Fujitani, Phys. Rev. B **62**, 4899 (2000).
[50]E. Artacho, D. Sánchez-Portal, P. Ordejón, A. Garcia, and J. M. Soler, Phys. Status Solidi B **215**, 809 (1999).
[51]J. Junquera, O. Paz, D. Sánchez-Portal, and E. Artacho, Phys. Rev. B **64**, 235111 (2001).
[52]E. Anglada, J. M. Soler, J. Junquera, and E. Artacho, Phys. Rev. B **66**, 205101 (2002).
[53]A. H. Larsen, M. Vanin, J. J. Mortensen, K. S. Thygesen, and K. W. Jacobsen, Phys. Rev. B **80**, 195112 (2009).
[54]A. Szabo and N. Ostlund, *Modern Quantum Chemistry* (MacMillan, New York, 1982).
[55]B. Delley, J. Chem. Phys. **92**, 508 (1990).
[56]G. Lippert, J. Hutter, P. Ballone, and M. Parrinello, J. Phys. Chem. **100**, 6231 (1996).
[57]M. A. Basanta, Y. J. Dappe, P. Jelínek, and J. Ortega, Comput. Mater. Sci. **39**, 759 (2007).
[58]D. J. Singh and L. Nordstrom, *Planewaves, Pseudopotentials, and the LAPW Method* (Springer, New York, 2006).
[59]C. H. Xu, C. Z. Wang, C. T. Chan, and K. M. Ho, J. Phys. Condens. Matter **4**, 6047 (1992).
[60]H. Haas, C. Z. Wang, M. Fähnle, C. Elsässer, and K. M. Ho, Phys. Rev. B **57**, 1461 (1998).
[61]D. Nguyen-Manh, D. G. Pettifor, D. J. H. Cockayne, M. Mrovec, S. Znam, and V. Vitek, Bull. Mater. Sci. **26**, 43 (2003).
[62]E. R. Margine, A. N. Kolmogorov, M. Reese, M. Mrovec, C. Elsässer, B. Meyer, R. Drautz, and D. G. Pettifor, Phys. Rev. B **84**, 155120 (2011).
[63]M. Mrovec, M. Moseler, C. Elsässer, and P. Gumbsch, Prog. Mater. Sci. **52**, 230 (2007).
[64]M. Mrovec, D. Nguyen-Manh, C. Elsässer, and P. Gumbsch, Phys. Rev. Lett. **106**, 246402 (2011).
[65]M. Reese, M. Mrovec, B. Meyer, and C. Elsässer, (unpublished).
[66]B. C. Carlson and J. M. Keller, Phys. Rev. **105**, 102 (1957).
[67]M. S. Tang, C. Z. Wang, C. T. Chan, and K. M. Ho, Phys. Rev. B **53**, 979 (1996); **54**, 10982(E) (1996).